JOURNAL OF GEOPHYSICAL RESEARCH, VOL. 114, E07001, doi:10.1029/2008JE003278, 2009

A hybrid model for leveed lava flows: Implications for eruption styles on Mars

Lori S. Glaze,[1] Stephen M. Baloga,[2] W. Brent Garry,[3] Sarah A. Fagents,[4] and Carolyn Parcheta[4]

Received 9 October 2008; revised 11 February 2009; accepted 30 April 2009; published 14 July 2009.

[1] Many channelized lava flows on the plains of Mars have substantial embanking margins and levees inferred to have been stationary while the central channel was active. Levee formation can be attributed to two end-member processes during emplacement: construction during passage of the flow front and growth along the entire length of the flow while it is active. It is shown here that the amount of lava that can be deposited by the flow front alone is limited. Estimates of the levee volume for many Mars plains flows exceed this limit and must have formed by processes that continued after the passage of the front. Experimental studies of analogous laboratory flows also indicate a combination of both modes of emplacement. A model that combines both modes of levee formation is presented, including a method for estimating volumetric flow rate, eruption duration, and viscosity. Six lava flows on the plains of the Tharsis volcanic province are used as illustrative examples. Crustal thicknesses for the six flows examined range from 9 to 23 m. Estimated emplacement times required to cool crusts of these thicknesses range from 1 year to 10 years. Corresponding viscosities are on the order of 10^5–10^6 Pa s. Effusion rates range from 25 to 840 m^3 s^{-1} and are all within the range of terrestrial observations. Therefore, the large leveed plains flows on Mars are not dramatically different in eruption rate or lava viscosity from large terrestrial analogs.

Citation: Glaze, L. S., S. M. Baloga, W. B. Garry, S. A. Fagents, and C. Parcheta (2009), A hybrid model for leveed lava flows: Implications for eruption styles on Mars, *J. Geophys. Res.*, *114*, E07001, doi:10.1029/2008JE003278.

1. Introduction

[2] Leveed lava flows have long been known to provide a unique opportunity to obtain inferences about their emplacement conditions [*Hulme*, 1974; *Carr*, 1974]. Many such flows on Mars, the Earth, and the Moon deposit a significant part of the active lava volume into stationary components, e.g., levees, margins, and stagnant zones (Figure 1). When the active and stationary components of the deposits can be distinguished, recently developed models of levee formation can be brought to bear that significantly diminish the need for unconstrained assumptions regarding lava rheology and emplacement time.

[3] Terrestrial observations [e.g., *Linneman and Borgia*, 1993; *Lipman and Banks*, 1987; *Moore*, 1987; *Guest et al.*, 1987, 1995] and laboratory experiments [e.g., *Garry*, 2006] indicate that levees and margins are established as the flow front passes (mode 1), and that additional contributions to the levees and margins continue long after the flow front has passed (mode 2). Specifically, the flow front leaves a stationary deposit along the margins of the flow to establish a channel, but subsequent overspills, clogs, and breakouts occur upstream, adding material to the levee. For lava flows on Mars, it is sometimes difficult to tell from morphology alone which of these two processes dominated levee formation (e.g., Figure 1). Even with recent advances in modeling, these two modes of levee and margin formation lead to significantly different quantitative inferences about emplacement conditions. Which end-member mode dominates the emplacement of a given flow affects quantitative estimates of volumetric flow rate, duration of emplacement, and rheology of the lava.

[4] These observations have motivated a new hybrid approach to levee formation during lava flow emplacement. In this work, the two modes of levee and margin formation are taken as end-members (Figure 2) that both affect lava flow emplacement to varying degrees. This new hybrid model for channelized lava flows builds levees and stationary margins by combining two time-dependent processes in two different zones along the flow length (Figure 3a). In the advancing Distal Zone, initial levees are constructed from the excess volumetric flow rate delivered to the flow front as described by *Baloga and Glaze* [2008]. This excess volumetric flow rate is due to the vertical velocity profile within the fluid inner core. As a result of the vertical velocity profile, upper laminae within the flow travel faster than the local average velocity. The excess volume flow rate

[1]NASA Goddard Space Flight Center, Greenbelt, Maryland, USA.
[2]Proxemy Research, Gaithersburg, Maryland, USA.
[3]Center for Earth and Planetary Studies, National Air and Space Museum, Smithsonian Institution, Washington, D. C., USA.
[4]Hawaii Institute for Geophysics and Planetology, University of Hawaii at Mānoa, Honolulu, Hawaii, USA.

0148-0227/09/2008JE003278$09.00

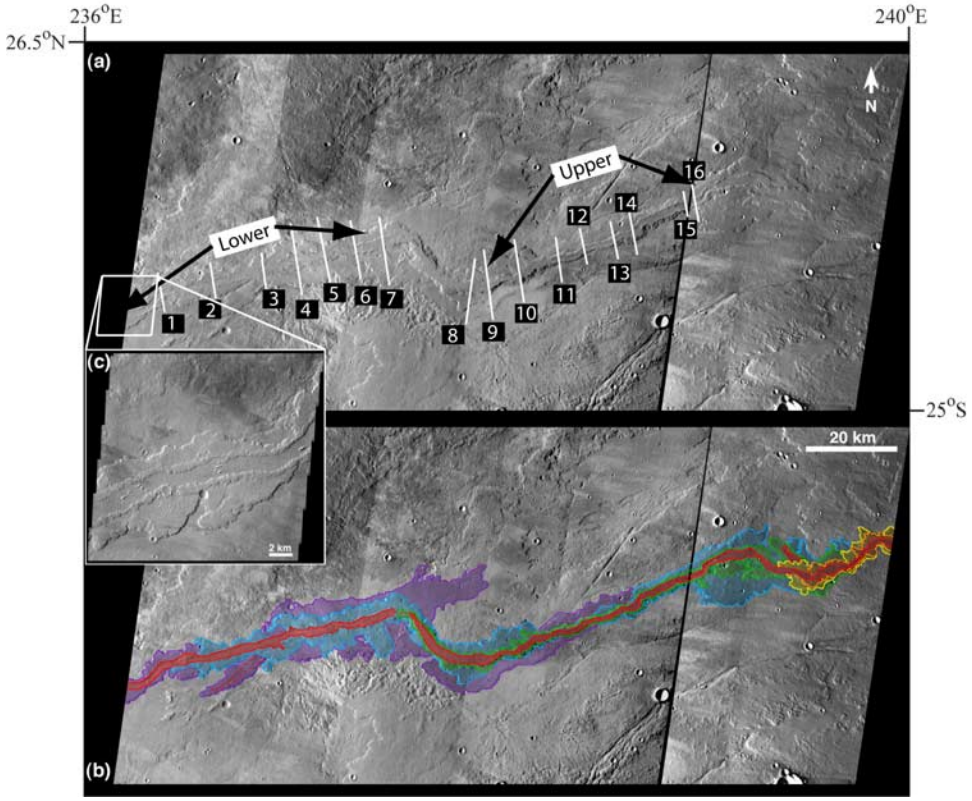

Figure 1. (a) Mosaic of Thermal Emission Imaging System (THEMIS) daytime infrared images (100 m pixel^{-1}) showing a 189 km long segment of a lava flow (flow 3 in Table 1 and Figure 7) in the Tharsis plains southwest of Alba Patera. Flow direction is from east to west (right to left). Cross-flow profile locations (white lines) and corresponding numbers refer to detailed measurement locations in Tables 4 and 5. (b) Coloration depicts central channel (red) and several generations of levees ranging in approximate order of youngest to oldest from orange, yellow, green, blue, and purple. (c) Inset is THEMIS Visible image V12686014 (37 m pixel^{-1}) showing detail of channel and levees.

may consist of deformable and nondeformable lava, and solid crust. To maintain an overall steady state and match with far-upstream conditions, the excess flow rate must be converted to stationary levees in the Distal Zone.

[5] As observed by *Rowland and Walker* [1990], in the fully developed steady state, far upstream Stationary Zone (Figure 3a), the average flow velocity generally exceeds the advance rate of the flow front. The difference in volumetric flow rate resulting from this velocity difference can produce a number of additional contributions to the margin and levee deposits in an Intermediate Zone (Figure 3a) through overspills, accretion, inward levee growth, local levee collapse, and small breakouts. The specific functional form presented here assumes that such processes, by definition, begin to occur once the distal levee building zone has passed. However, these processes must eventually decay with distance from the flow front to match asymptotically with the upstream steady state conditions in the Stationary Zone. The model presented here only uses the cumulative (integrated) volume deposited in the Intermediate Zone. Therefore, it is not sensitive to the detailed functional form of these secondary mechanisms for margin and levee growth behind the advancing flow front.

[6] Here, the motivation for the hybrid approach is described by presenting a specific Mars example and experimental results. Limits are then identified on the range of levee volumes that can be explained by the *Baloga and Glaze* [2008] approach to levee formation only at the flow front (from a combination of excess flow volume and crust). When the volume of lava contained in the levees exceeds this amount, some other process must be adding levee volume upstream. A theoretical approach is proposed for "bleeding" off part of the excess volume flow rate locally and continuously (as the simplest assumption) along the path of the flow. The problem is then to find how much more volume is contained in the levees as a function of the difference between the front velocity and the average velocity in the Stationary Zone. Examples are provided to demonstrate the range of results for six long leveed flows on the plains of the Tharsis region of Mars.

2. Motivation for the Hybrid Approach

[7] Many authors have investigated leveed lava flows [e.g., *Hulme*, 1974; *Zimbelman*, 1985; *Baloga*, 1987; *Crisp and Baloga*, 1990; *Baloga et al.*, 1998, 2003; *Rowland et al.*, 2004; *Glaze and Baloga*, 2006; *Garry et al.*, 2007; *Baloga and Glaze*, 2008]. To simplify the physics, the early studies took the existence of a channel as a given. This assumption ignores the interaction between the dynamics in the channel and the growth of the levee. The formation of stationary margins implies that some volume of lava must

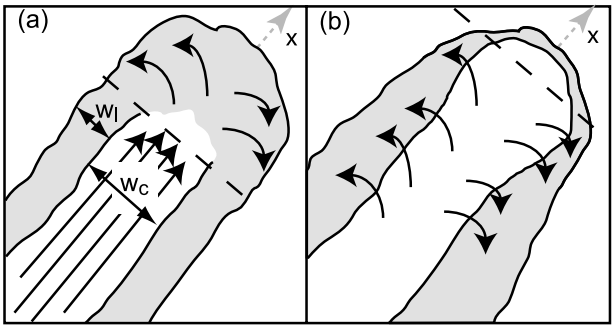

Figure 2. Cartoon illustrating the two end-member processes for forming lava flow levees: (a) through deposition of excess volume flow rate and crust as the flow front passes and (b) through inward growth and/or overspills after the flow front has passed. Flows are advancing in the *x* direction. Levee and channel widths corresponding to the *Baloga and Glaze* [2008] model described in equations (1)–(7) are denoted in Figure 2a by w_l and w_c, respectively.

be transferred from the active, flowing channel to the stagnant margins through levee building near the flow front, along the length of the flow, or through small upstream breakouts and overspills. Such processes are common in terrestrial basalt flows [e.g., *Lipman and Banks*, 1987; *Rossi*, 1997; *Bailey et al.*, 2006]. Over the last decade, several theoretical studies have begun to address the impact of the levee formation process on lava flow emplacement dynamics [*Baloga et al.*, 1998, 2003; *Glaze and Baloga*, 1998, 2006; *Baloga and Glaze*, 2008].

[8] *Baloga et al.* [1998] developed an approach that transfers lava volume from the active channel to stagnant levees throughout the duration of emplacement via the end-member process illustrated in Figure 2b. This model assumes that once the flow front has passed, lava is continuously transferred into the stationary margins. In this first attempt, the transfer rate was assumed to be constant at all points along the flow. However, this approach predicts levees that should be narrow toward the flow front, and relatively wide near the vent. This is not consistent with observations. *Glaze and Baloga* [2006] extended this approach to consider a variable rate of lava transfer. In this case, material is still continuously transferred to stationary margins after the flow front has passed, however, the rate at which material is transferred increases as a function of distance. This allows for more uniform levee dimensions along the length of a flow. While the *Glaze and Baloga* [2006] model works well for some flows, there are some instances where the model results do not seem to agree well with data [*Baloga and Glaze*, 2008].

[9] Recently, *Baloga and Glaze* [2008] developed a completely new approach to modeling levee formation, along the lines of the end-member process illustrated in Figure 2a, that transfers lava from the active channel into stagnant margins only at the flow front. This type of process appears to occur during the emplacement of many long channelized lava flows on the Mars plains that exhibit a self-replicating nature, i.e., those with more or less the same relative dimensions, morphology, and appearance at all points along the flow path. Self-replication implies a more-or-less steady state supply of lava at the vent for protracted periods of time. In this end-member process, once the flow front has passed, the levees then cease to grow. The volume of material transferred into the margins at the flow front is determined by the excess flow velocity (velocity of material moving faster than the average advance rate of the flow) in the channel. Any levee volume that cannot be accounted for with excess velocity in the fluid core is assumed to come from a nondeformable or solid crust that is also deposited at the flow front.

[10] Although results of the *Baloga and Glaze* [2008] model for self-replicating flows are encouraging on the basis of application to a long lava flow north of Pavonis Mons [*Baloga and Glaze*, 2008], many instances occur where the self-replication model seems to fail for long (>100 km) lava flows in the Mars plains. This comes as a surprise, because these flows appear to exhibit characteristics of self-replicating flows as defined by *Baloga and Glaze* [2008]. The key issue with most of these flows is that the observed levee volumes require far more lava than could have come from the combination of excess flow velocity and crust deposition solely by the flow front.

[11] *Baloga and Glaze* [2008] assume a Newtonian rheology within the fluid core of a lava flow. The core can be covered by a layer of nondeformable lava, hereafter referred to as 'crust'. In the *Baloga and Glaze* [2008] model, there are only two longitudinal zones in the lava flow, an upstream steady state channel in the Stationary Zone and a time-dependent Distal Zone (Figure 3). Levee building occurs exclusively in the Distal Zone (there is no Intermediate Zone as defined in Figure 3). Levee dimensions are determined by the volumetric flow rate in the upper (vertically) portion of the flow in the Stationary Zone that is greater than the average flow rate of the inner molten core. The key assumption of the *Baloga and Glaze* [2008] model is that the flow front advances at the same rate as the average velocity of the channel zone. Within the molten core in the Stationary Zone, the vertical velocity profile for a Newtonian fluid is (see notation)

$$u_c(z) = \frac{\rho g \sin\theta z}{\mu}\left(h_c - \frac{z}{2}\right) \tag{1}$$

From the combined deformable and nondeformable layers, the excess volumetric flow rate that must go into the levee building in the Distal Zone was shown by *Baloga and Glaze* [2008] to be

$$Q_{ex} = Q_{ex:core} + Q_{ex:crust} = \bar{u}_c w_c\left[\frac{h_c}{3\sqrt{3}} + \frac{1}{2}(h_l - h_c)\right] \tag{2}$$

where w_c is the width of the channel (Figure 2a), h_c is the thickness of the actively flowing lava core within the channel, and h_l is the thickness of the fluid core plus any solid nondeformable crust that is riding on top. This excess volume flow rate is assumed to construct a triangular levee on each side of the flow. From (2), the width of the levee can be shown to be

$$w_l = \frac{Q_{ex}}{\bar{u}_c h_l} = \frac{w_c}{h_l}\left[\frac{h_c}{3\sqrt{3}} + \frac{1}{2}(h_l - h_c)\right] \tag{3}$$

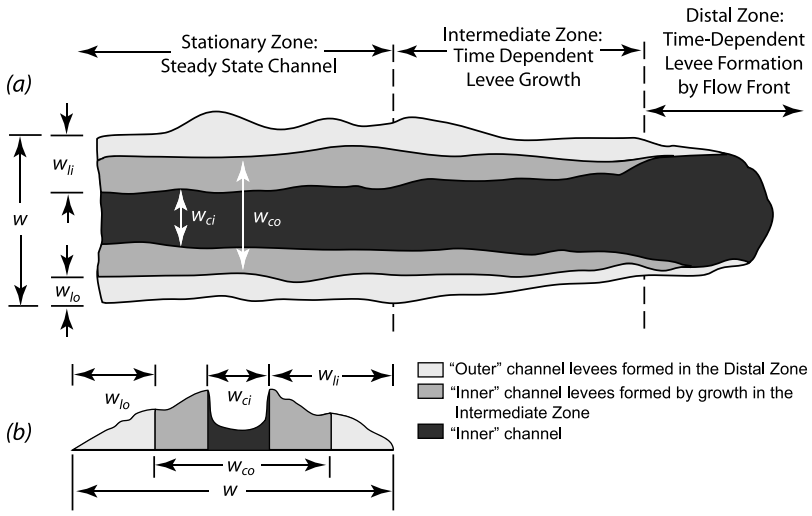

Figure 3. (a) Cartoon illustrating the three zones of the hybrid model. In the Distal Zone, volume is transferred from the active channel to the stagnant levees at the flow front (light gray). In the time-dependent Upstream Zone, lava is continuously added to the levees through inward growth and/or small overspills (medium gray). In the far upstream Stationary Zone, the channel (darkest gray) has reached a steady state and the levees no longer increase in volume. (b) Cartoon of terminal cross-flow deposit profile showing definitions of measured variables used for actual flow applications. See notation for variable definitions. The inner channel is taken to be the final observed channel. Inner and outer channel and levee dimensions are used directly in equations (8), (17), and (19).

where w_l is the width of the levee (on one side, see Figure 2a). Using measured dimensions of the channel and levees, (3) can be solved for molten core and crust thicknesses. The crust thickness provides the constraint on emplacement time when supplemented independently by a cooling law [*Hon et al.*, 1994]. Once this is known, the core thickness provides, in essence, the constraint on the core viscosity. Details of the derivation of the excess volumetric flow rate are provided by *Baloga and Glaze* [2008].

[12] If the assumptions required for the original self-replication hypothesis are satisfied, there are limits to the dimensions of levees that can be constructed in the Distal Zone. Admissible limits on the dimensions of the flow, the levees, and the thickness of the overriding crust are obtained by noting that the core height must lie in the range from 0 to h_l. At one end of this range, the lava within the channel is all crust with essentially no moving deformable core. In this case, for $h_c = 0$, (3) gives

$$w_l = \frac{w_c}{2} \tag{4}$$

At the other end of the range, when $h_c = h_l$, there is no crust and (3) becomes

$$w_l = \frac{w_c}{3\sqrt{3}} \tag{5}$$

Thus, the allowable range of w_l (where the thickness of the active channel core is by definition less than the total flow thickness) for a flow generating levees only at the front is given by

$$\frac{w_c}{3\sqrt{3}} \le w_l \le \frac{w_c}{2} \quad \text{for} \quad h_l \ge h_c \ge 0 \tag{6}$$

[13] To satisfy the conditions in (6), the channel must be wide relative to the levee width. Often, however, flows are observed that appear to have narrow channels relative to the overall flow width, indicating a disproportionately large volume of lava in the levees. One such example is a very long flow on the distal flanks southwest of Alba Patera. Figure 1 shows a 189 km long section of this lava flow extending from 25.9°N, 239.4°E to 25.4°N, 236.2°E in the plains between Olympus Mons and Alba Patera. Neither the flow source nor the terminus is observed in the Thermal Emission Imaging System (THEMIS) visible and infrared data. However, the flow direction can be determined on the basis of topography and flow morphology. The general downhill trend is from east to west, and the morphologies of overspills are also consistent with flow from east to west. The final channel, active during the last phases of the eruption, is shown in red. Several generations of levees can be identified along the flow. The different generations were distinguished from one another by their superposition relationships and observations of apparent channel breaches and/or overspills. For the section shown in Figure 1, the levees are delineated, in approximate order of increasing age, by orange, yellow, green, blue, and purple margins. However, in locations where multiple generations of levees are not present, it is not always possible to determine relative ages for all levees. There is some morphologic evidence of self-replicating behavior, primarily the fact that this flow is >189 km long with a sustained channel that did not appear to experience sufficient surges or drops in flow rate to cause major breakout lobes. Midway along the flow where it turns to the northwest, the flow appears to have ponded and possibly stagnated for an indeterminate period. Here the topographic slope has shallowed relative to the reaches above and below this segment. This is a complex segment of the flow with significant ambiguity in the time

Table 1. Average Flow Dimensions for Flows Shown in Figure 7[a]

Flow	Name	L (km)	w (km)	Inner w_c (km)	Outer w_c (km)	θ (deg)	h_l (m)
1	Pavonis West	307	33.7 ± 5	9.2 ± 1.9	19.7 ± 3.2	0.09	31 ± 4
2	Pavonis East	173	26.7 ± 3.8	8.3 ± 1.3	16.3 ± 2.8	0.07	49 ± 5
3	Alba (Upper)	53	9.9 ± 0.8	4.9 ± 1.2	6.4 ± 0.8	0.51	25 ± 5
3	Alba (Lower)	48	11.0 ± 2.6	4.3 ± 0.5	7.6 ± 1.4	0.51	42 ± 4
4	Arsia North	75	4.7 ± 0.7	1.5 ± 0.3	2.9 ± 0.5	0.70	23 ± 5
5	Arsia Southeast[b]	146	3.6 ± 0.7	1.0 ± 0.2	2.1[b]	0.85	20 ± 4
6	Arsia Southwest[b]	158	4.7 ± 1.4	0.9 ± 0.3	2.5[b]	0.60	28 ± 4

[a]Uncertainties correspond to 2 times the standard error on the mean. Detailed data used to derive these statistics are provided in Tables 2–8.
[b]Outer channel dimensions for these two flows are estimates based on the average relationship between inner and outer levee width for the other four flows. See text for explanation.

sequencing of the levee and margin deposits. Here, it is difficult to extract the dimensional data needed to apply the hybrid levee model. In the analysis below, the segments above and below this intermediate reach are treated separately.

[14] On the basis of the final channel shown in red in Figure 1, the average channel widths (see Inner w_c data for flow 3 in Table 1) in the upper (proximal) and lower (distal) reaches of this flow are w_c = 4.9 km ± 1.2 km and w_c = 4.3 km ± 0.5 km, respectively, with corresponding levee widths of w_l = 3.4 km in both segments. According to (6), if levees are generated at the flow front alone, the ratio of levee width to channel width in each of the flow segments must lie in the range such that

$$0.19 \leq \frac{w_l}{w_c} \leq 0.5 \tag{7}$$

However, the width ratios of 0.7 for the upper reach and 0.8 for the lower reach are both well beyond the acceptable range defined in (7) for formation solely by deposition at the flow front.

[15] In addition to the issues related to overall levee volume compared to channel volume, cross-flow topographic profiles for some flows (e.g., Figure 4) seem to indicate that levees may have formed in multiple stages. Several flows exhibit what appear to be channel widths that varied over time, e.g., an early "wide" channel, followed by a "narrow" channel toward the end of the eruption. The profile shown in Figure 4 is interpreted in the following way. As the flow front passed this point, the "outer" levees were emplaced. After the flow front had passed, the levees continued to grow inward, with material removed from the active "inner" channel and deposited into the "inner" channel levee as identified in Figure 4.

[16] The flow shown in Figure 1 exhibits evidence for such stages of levee growth. The outermost (interpreted as oldest) levees for this flow (blue or purple in Figure 1b) indicate a possible early outer channel with w_{co} = 6.4 ± 0.8 km and w_{lo} = 1.8 km in the upper reach, and w_{co} = 7.6 ± 1.4 km and w_{lo} = 1.4 km in the lower reach. The ratio of levee to channel width for the upper reach of the Alba flow is 0.28, well within the range defined by (7). However, the width ratio for the lower reach is 0.18, just below the lower limit in (7), i.e., the margins in the lower reach are too narrow to be explained by the transfer of excess volume into levees at the flow front. In this case, much of the lower reach appears to have been emplaced by some process other than self replication and the flow front levee emplacement model is not appropriate.

[17] Flows such as the upper reach of the flow in Figure 1, and the flow from which the topographic profile in Figure 4 was taken (flow 1 in Table 1), suggest the need for a hybrid levee formation approach that combines both end-member processes. For this hybrid approach, excess velocity at the flow front transfers lava volume and overriding crust to stagnant margins. Then, after the flow front passes, the levees continue to grow until they reach an asymptotic limit. Once the levees have stabilized (ceased to grow), the lava in the active channel establishes a steady state.

[18] Similar multistage levee formation is also seen in laboratory experiments using polyethylene glycol (PEG) which is a common material for simulating lava flow morphologies [e.g., *Fink and Griffiths*, 1990; *Gregg and Fink*, 1995, 1996; *Blake and Bruno*, 2000; *Griffiths et al.*, 2003; *Cashman et al.*, 2006; *Garry et al.*, 2006, 2007; *Kerr et al.*, 2006]. The PEG experiment shown in Figure 5 used different colored waxes to illustrate levee formation as a function of time [*Garry*, 2006]. The laboratory setup fol-

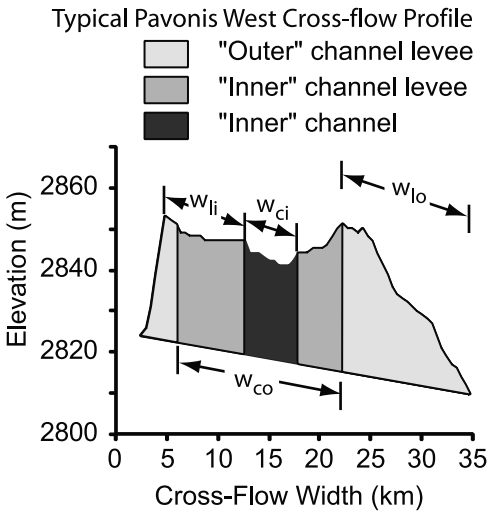

Figure 4. Typical cross-flow profile of the Pavonis West (flow 1 in Table 1 and Figure 7) lava flow. Elevations are taken from MOLA gridded data (128 pixels degree^{-1}). Evidence of at least two periods of levee growth can be seen. The light gray region represents levees that likely formed in the Distal Zone as the flow front passed. The medium gray region indicates additional inward levee growth, and the darkest gray represents the final channel that can be observed in visible images of this flow.

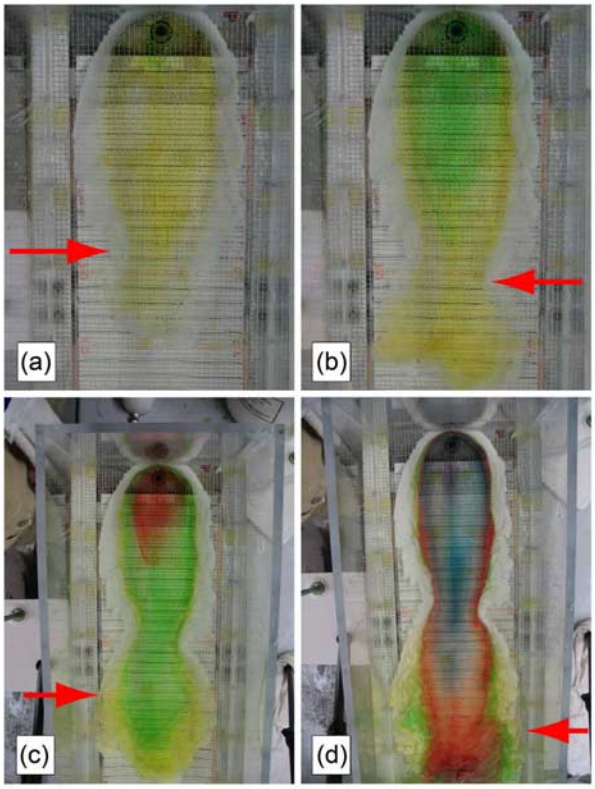

Figure 5. Development of a channelized polyethylene glycol (PEG) flow. Red arrows indicate the maximum longitudinal extent of solidified levees. Total experiment duration from initial effusion until the vent was plugged was 310 s. Colored dyes added to the originally clear PEG effused from the vent at the following times: white (0 s), yellow (57 s), green (98 s), red (170 s), blue (280 s). (a) Solidification of the initial levees along the first 26 cm of the flow length (110 s). (b) Levees extend 30 cm from the vent. Distal Zone of flow spreads laterally (136 s). (c) Levees extend ~36 cm from the vent (182 s). (d) Channel and levees develop along 60 cm of flow length, but the stability of the levee construction changes along the flow length (293 s). The tank is 70 cm long. Black lines on the floor are spaced 2 cm. A wire mesh screen is placed along the tank floor to prevent slippage of the PEG on the Plexiglas. Underlying slope is 6°. Experiment BG-115 from *Garry* [2006].

lowed that of *Fink and Griffiths* [1990]. This particular channeled flow (BG-115) was formed by pumping warmed PEG (24.5°C) at a constant rate (4.77 mL sec^{-1}) into a tank (70 cm long, 28 cm wide) set at underlying slope of 6° that was filled with a chilled sucrose solution (13°C). The Plexiglas floor has a wire mesh to prevent slippage of the wax, and the vent was plugged after 310 s. The final flow thickness was 0.6–0.7 cm. The experiment was held at a constant effusion rate, consistent with self-replicating flows and analogous to the steady state assumption used by both end-member models. This scenario shows development under constant and idealized parameters that can be extrapolated to terrestrial levee development regardless of material or flow length [*Garry*, 2006]. The growth of the channel-levee system with time shown in Figure 5 is based on the color distribution of the liquid and solid PEG, which is clear in liquid form and white when solid (PEG solidifies at ~18.5–20.0°C). Different colored dyes were added to the source bucket of PEG in ~60 s time intervals (yellow, green, red, and blue). The white portions of the levees were emplaced as the flow front passed. The yellow, green and red portions of the levees visible along the first 30 cm of the flow length from the vent were formed by inward levee growth after the flow front had passed and the levees were well established.

3. Hybrid Model

[19] Here, a new quantitative approach is presented for describing levee and stationary margin construction by a combination of the two end-member processes shown in Figure 2. To begin, it is assumed that the volume flow rate at the vent is constant and that some volume of lava is transferred to the stationary margins as the flow front passes. Assuming that the outer channel levee (as defined in Figures 3 and 4) was emplaced as the flow front passed, (3) can be rewritten and solved for the thickness of the active lava core in terms of measurable dimensions for the outer channel, the outer channel levee, and the total flow thickness:

$$h_c = \frac{h_l\left(\frac{w_{lo}}{w_{co}} - \frac{1}{2}\right)}{\left(\frac{1}{3\sqrt{3}} - \frac{1}{2}\right)} = 0.213h_l\left(\frac{w_{lo}}{w_{co}} - 0.5\right) \tag{8}$$

[20] Once (8) has been solved for the thickness of the active core, the crust thickness, $h_l - h_c$, can be found. As was done by *Baloga and Glaze* [2008], the time to grow a crust of this thickness by conductive cooling [*Hon et al.*, 1994] is taken as an estimate of the time of emplacement for the flow over the reach observed. The average advance rate of the flow front, u_f, is defined as the total lava flow length divided by the emplacement time.

[21] If the flow front advance rate, u_f, is less than the far upstream steady state velocity, $\bar{u}_c$, additional lava volume excess different from that described by *Baloga and Glaze* [2008] is available after the flow front passes, along the existing path of the lava channel. *Rowland and Walker* [1990] noted this difference between the velocity of lava in the upstream channel and the slower advance rate of the flow front. This excess velocity can cause overspills upstream or inward levee growth, both of which increase the volume in the stationary margins beyond the upper limit indicated by (6).

[22] To first order, the channel flow depth for most flows observed on the plains of Mars is relatively constant [e.g., *Zimbelman*, 1985; *Mouginis-Mark and Yoshioka*, 1998; *Glaze and Baloga*, 2007; *Baloga and Glaze*, 2008]. Keeping the volumetric flow rate at the vent constant over time, a general expression for the transfer of lava volume from the active channel to stationary margins in the Intermediate Zone (Figure 3a) can be obtained. Considering only this process of levee formation (Figure 2a), and for two symmetric triangular shaped levees of height h_l, volume conservation is expressed by

$$2\left(\frac{1}{2}\right)\int_{o}^{L(t)} w_l(x,t)dx = \bar{u}_c t w_c(0) - \int_{0}^{L(t)} w_c(x)dx \tag{9}$$

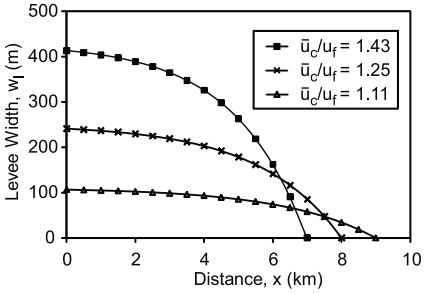

Figure 6. Plot illustrating how the levee width increases as the difference between the average channel velocity and advance rate increases. The plot assumes two symmetric triangular shaped levees are constructed on each side of the flow. All three curves assume t = 10,000 s, Γ = 3000 s, w_c = 1000 m, and u_c = 1 m s^{-1}. The three cases shown correspond to advance rates at the flow front of u_f = 0.9 m s^{-1} (triangle), 0.8 m s^{-1} (cross), and 0.7 m s^{-1} (square).

The left hand side of (9) is simply the accumulated excess volume in the levees due to the difference (on the right hand side) between the velocity in the upstream channel and the velocity at which the flow is advancing at the front. When these two velocities are equal, there is no excess volume upstream and levees are constructed only in the Distal Zone. For a constant channel width,

$$\int_o^{L(t)} w_l(x,t)dx = [\bar{u}_c t - L(t)]w_c \tag{10}$$

In principle, w_l could be highly variable as long as the integral remains the same. However, it would make no sense in view of the other assumptions (e.g., constant advance velocity) to have the variations be large.

[23] A plausible model for levee growth in the Intermediate Zone allows the levee volume at each location along the flow path to increase with time after the flow front passes, but not indefinitely. At some time (constrained by a time constant Γ), the channel stabilizes and the levees cease to grow. If the final levee width is given by w_∞, a reasonable expression for this asymptotic levee growth with time can be written as

$$w_l(x,t) = w_\infty\left(1 - e^{-t/\Gamma(1-x/L))}\right) = w_\infty\left(1 - e^{-t/\Gamma + x/u_f\Gamma}\right) \tag{11}$$

where $L(t) = u_f\, t$ in the last expression on the right hand side, indicating an average advance rate of the flow front, u_f.

[24] Using the form in (11) for levee growth, and again letting $L(t) = u_f\, t$, (10) becomes

$$\int_o^{u_f t} w_l(x,t)dx = w_\infty \int_o^{u_f t}\left[1 - e^{-t/\Gamma(1-x/L)}\right]dx = \left(\bar{u}_c t - u_f t\right)w_c \tag{12}$$

Evaluating the integral in (12),

$$1 - \frac{\Gamma}{t}\left(1 - e^{-t/\Gamma}\right) = \frac{w_c}{w_\infty}\left(\frac{\bar{u}_c}{u_f} - 1\right) \tag{13}$$

Solving for the flow velocity in the Stationary Zone,

$$\bar{u}_c = u_f\left[1 + \frac{w_\infty}{w_c}\left(1 - \frac{\Gamma}{t}\left(1 - e^{-t/\Gamma}\right)\right)\right] \tag{14}$$

Thus, for long times ($t \gg \Gamma$), allowing the channel to stabilize,

$$\bar{u}_c = u_f\left(1 + \frac{w_\infty}{w_c}\right) \tag{15}$$

[25] Solving (15) for w_∞ (final levee width resulting from growth after the flow front has passed), and substituting into (11), an expression for w_l (x, t) can be found as a function of the difference between the steady state velocity in the Stationary Zone and the advance rate in the Distal Zone:

$$w_l(x,t) = w_c\left(\frac{\bar{u}_c}{u_f} - 1\right)\left(1 - e^{-t/\Gamma + x/u_f\Gamma}\right) \tag{16}$$

[26] Figure 6 provides a quantitative example of how the difference between the channel and advance velocity affects the width of the levee. Figure 6 shows w_l at time t = 10,000 s, and Γ = 3,000 s. In all three examples, w_c = 1000 m, and the velocity of lava in the Stationary Zone channel is 1 m s^{-1}. As the advance rate of the flow front decreases from 0.9, to 0.8, to 0.7 m s^{-1}, the levee width increases systematically. Thus, adjusting the difference between the channel and advance velocities provides a mechanism for explaining levee volumes exceeding those admissible by the distal construction process.

[27] Equation (15) can be recast in a form directly applicable to the dimensional measurements of channelized lava flows with the following definitions (see Figure 3). The outer levee width is the distance from the highest point on the levees emplaced by the passage of the front to the outer margin of the flow. The inner levee width is defined to be the distance from the margin of the final observed channel to the outer margin of the flow. The reason for defining the inner levee in this way is that it is most consistent with dimensions that can be measured from image and topographic profile data. With these definitions, $w_\infty = w_{li} - w_{lo}$. Thus, when the inner and outer levees can be discerned, these dimensions constrain the difference in the two advance rates:

$$\bar{u}_c = \left(1 + \frac{w_\infty}{w_c}\right)u_f = \left(1 + \frac{w_{li} - w_{lo}}{w_{ci}}\right)u_f \tag{17}$$

For the expression in (17), w_∞ corresponds to the volume of lava in the levees associated only with growth after the flow front has passed.

[28] For a Newtonian fluid, once the velocity of lava in the Stationary Zone channel is known, the dynamic viscosity is then

$$\mu = \frac{\rho g \sin\theta h_c^2}{3\bar{u}_c} \tag{18}$$

and the volume flow rate at the vent for each flow is simply

$$Q = h_l \bar{u}_c w_{ci} \tag{19}$$

4. Model Applications

[29] The new hybrid model has been applied to six lava flows on the relatively flat plains of the Tharsis volcanic region (Figure 7). These flows range in length from 50 to 300 km, and have thicknesses of 20–50 m. Emplacement slopes are all less than 1°. These six flows were chosen for analysis because all the necessary data have either been published previously or were already in hand. Some of the methods for determining dimensions may vary, but the basic dimensional data satisfy the requirements of the hybrid model. The levees of flow 2 have already been examined by several studies [*Baloga et al.*, 2003; *Glaze and Baloga*, 2006, 2007; *Baloga and Glaze*, 2008]. Flows 1 and 4 were also examined by *Glaze and Baloga* [2007]. Flow 3 is shown in Figure 1, and flows 5 and 6 were examined by *Garry and Zimbelman* [2007]. Dimensional measurements of flow thickness, channel width and levee width for flows 1, 2, 5 and 6 were determined from the Mars Orbiter Laser Altimeter (MOLA) gridded data (128 pixels degree^{-1}) [see *Smith et al.*, 2001]. Dimensional data for flows 3 and 4 were determined from individual MOLA Precision Experiment Data Record (PEDR) profiles. Note that as only the upper reach of flow 3 appears consistent with the self-replication model, the lower reach is not considered in the subsequent analyses. Average dimensions for each of the flows analyzed here are contained in Table 1 and the detailed measurements are provided in Tables 2–8.

[30] For flows 1–4 (Pavonis West, Pavonis East, Alba (Upper), and Arsia North), there is relatively clear evidence of "inner" and "outer" levees as illustrated by the Pavonis West profile in Figure 4. For flows 5 and 6, dimensions were taken directly from *Garry and Zimbelman* [2007], where channel widths were only determined for the inner channel. To estimate what the outer channel and levee dimensions might be, we examined the ratios of inner to outer widths for the levees and channels of flows 1–4 (Table 9). The ratio of levee widths (w_{lo}/w_{li}) for these four flows show less variability than the channel widths (w_{ci}/w_{co}), i.e., the standard deviation is smaller (see Table 9). Therefore, the averaged ratio of levee widths, equal to 0.58, has been used to estimate the outer levee widths for flows 5 and 6 ($w_{lo} = w_{li} \times 0.58$). The outer channel widths for flows 5 and 6, given in Table 1, are then found by $w_{co} = w - 2 \times w_{lo}$.

[31] The first step in the hybrid approach is to estimate the thickness of the crust that must have been deposited in the outer levees as the flow front passed. In some cases, such as flow 2, detailed information is available on the dimensions of the flow at several positions along the length of the flow [*Baloga and Glaze*, 2008]. More commonly, however, only averaged flow dimensions are available in the published literature. Therefore, we first demonstrate that these averaged, representative, flow dimensions can be used in the hybrid model if more detailed data are not available. To make this comparison, two computations of the crust thickness were made. The first method for estimating the crust thickness is similar to what is described by *Baloga and Glaze* [2008], taking advantage of the full, detailed measurements of flow dimensions at multiple locations along the flow path. The second method simply calculates the crust thickness for a single set of averaged flow dimensions.

[32] The first method attempts to use all of the detailed cross-flow MOLA topographic data. However, in most cases, there are some locations along the flow length with outer channel and levee widths that do not satisfy the criterion defined in (6), indicated by bold type in Tables 2–8. These locations are generally associated with assignable causes that include sudden changes in channel width, major outbreaks and overspills, and late stage inward levee growth beyond the time scale of relevance for this model. Core thicknesses cannot be determined at such locations. For those locations with w_l/w_c dimensions that do satisfy the criterion in (6), flow dimensions are used to determine the core thickness from (8). The crust thickness is then simply $h_l - h_c$ at that location. Although there is a great deal of variability between stations, the average of these values is taken as the best estimate for the crust thickness for the entire flow.

[33] As an alternative to calculating the core thickness at each station and then averaging, representative dimensions for each flow can be used to calculate the average core thickness directly. To demonstrate the utility of this averaged approach, core thicknesses have been calculated using both approaches for flows 1–4: Pavonis West, Pavonis East, Alba (Upper), and Arsia North. For these four flows, the representative values for flow thickness (h_l), outer channel width (w_{co}) and outer levee width (w_{lo}), were all estimated by taking an average of those measured values at stations that pass the criterion in (6). These averaged flow and channel dimensions are contained in Table 1. Uncertainties are associated with the 95% confidence interval (2 times the standard error on the mean).

[34] Table 10 compares the crust thicknesses estimated by the two averaging approaches (using the full data set and from averaged dimensions). On the basis of the results shown in Table 10, crust thicknesses found by averaging the flow dimensions first are similar to those derived from the more complex, complete flow dimension data set. Thus, the rest of the discussion presented here is based on only the analysis of average flow dimensions (given in Table 1).

[35] Once the crust thickness has been determined, this thickness can be associated with emplacement time. Following *Baloga and Glaze* [2008], it is assumed that the time required to solidify a crust (thicknesses given in Table 10) is approximately the amount of time for the flow to be emplaced. The simplest approach to estimating this time is to assume that the crust cools owing to conduction [*Hon et al.*, 1994]. These times are given in Table 11.

[36] The advance rate of the flow front is found by dividing the total length of the flow that can be distinguished in image data by the emplacement time. Using the average dimensions of the inner channel (Table 1), the channel velocity can be estimated from (17), the viscosity from (18), and the effusion rate at the vent from (19). Table 11 shows the results for each flow. For comparison, *Moore* [1987, Table 58.5, station 1] found channel velocities of 2–4 cm s^{-1} in the lower reach of the basaltic 1984 Mauna Loa 1A flow where the flow was 4–9 m thick, and viscosity at station 1 was estimated to be 10^5 Pa s. It is worth noting that

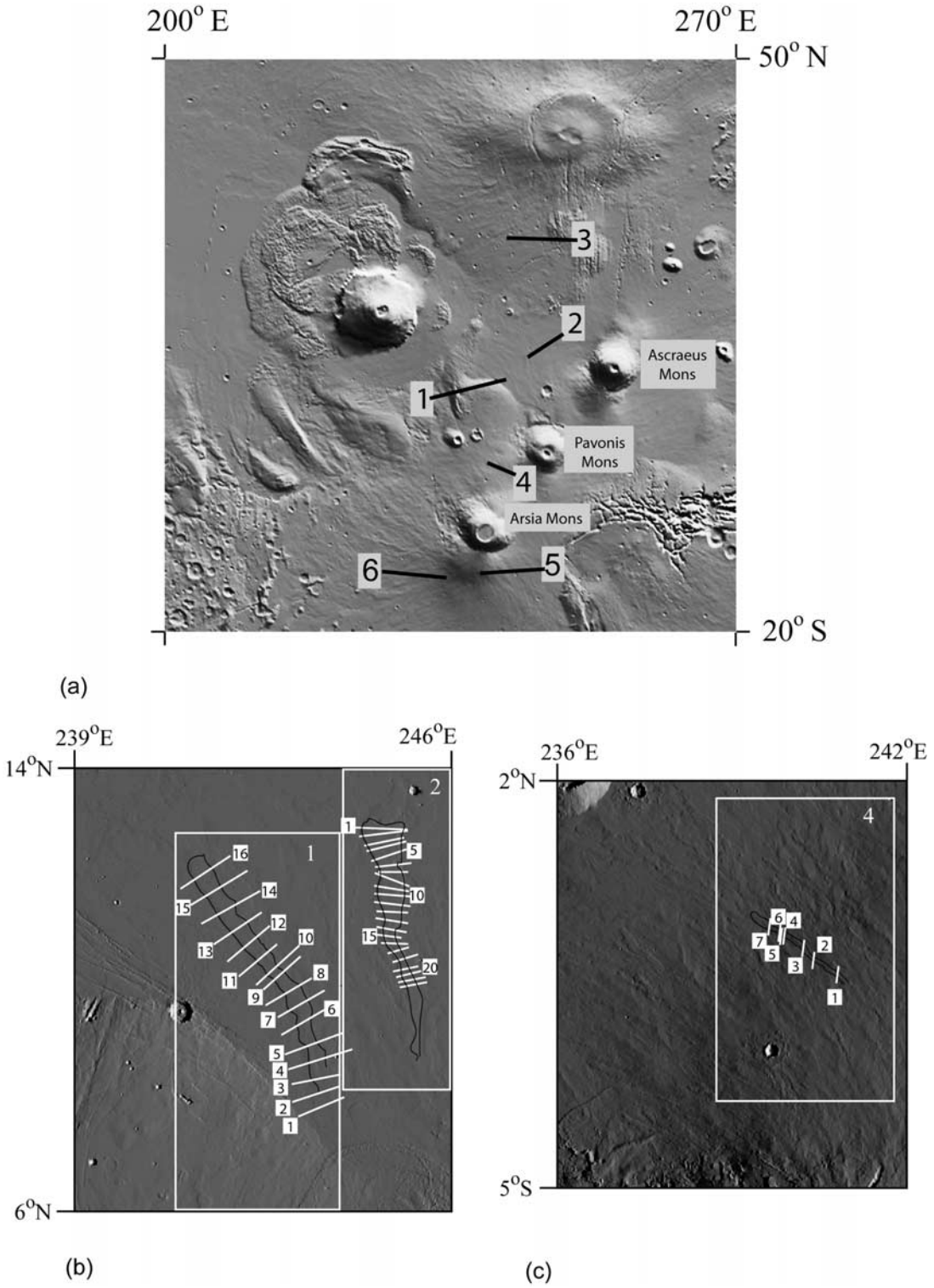

Figure 7. (a) Shaded relief context map derived from gridded MOLA data (128 pixels degree^{-1}) indicating locations of the six flows studied here. Detailed locations are also shown for (b) flow 1 (Pavonis West) and flow 2 (Pavonis East) (on shaded relief representation of gridded MOLA data), (c) flow 4 (Arsia North) (on shaded relief representation of gridded MOLA data), (d) flow 5 (Arsia Southeast) (on THEMIS IR mosaic from THEMIS daytime IR map with 231.55 m pixel^{-1} resolution), and (e) flow 6 (Arsia Southwest) (on THEMIS IR mosaic from THEMIS daytime IR map with 231.55 m pixel^{-1} resolution). Cross-flow profile locations (white lines) in Figure 7b–7e, and corresponding numbers, refer to detailed measurement locations in Tables 2, 3, 6, 7, and 8, respectively. Locations of cross flow profiles for flow 3 (Alba Upper and Lower) are shown in Figure 1 and corresponding measurements are provided in Tables 4 and 5.

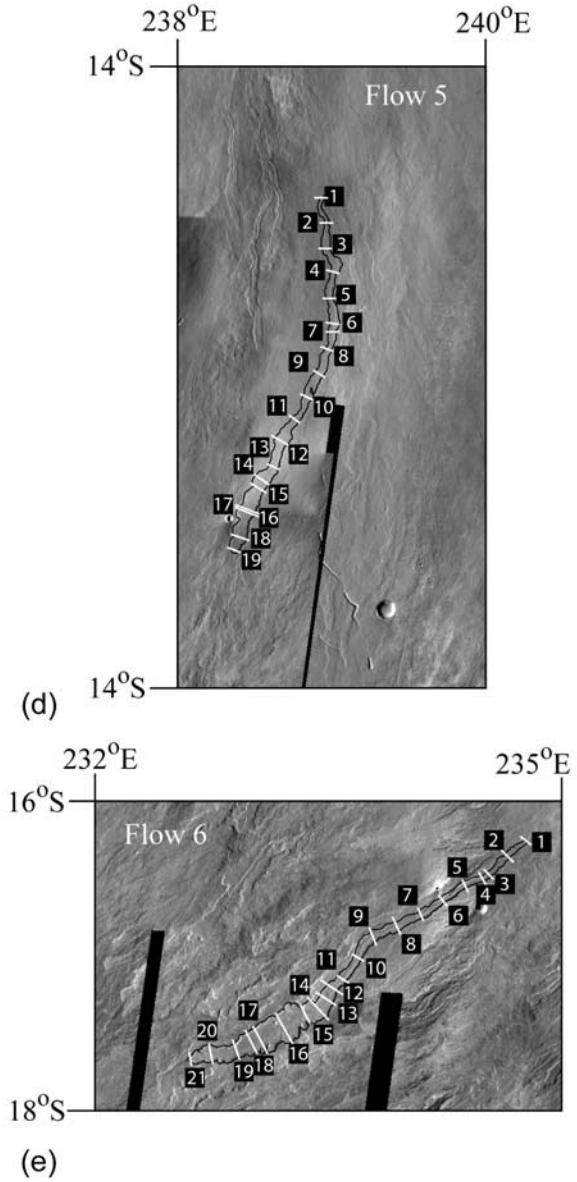

Figure 7. (continued)

upstream, channel velocities were 1–2 orders of magnitude higher [*Moore*, 1987, Tables 58.2 and 58.3, stations 4 and 8]. Given that the ~3.3° slope in this lower reach of the 1A flow was significantly higher than for the Mars plains flows, it is reasonable to expect lower channel velocities for the Mars flows. Alternatively, lower channel velocities on Mars might be explained by more viscous (possibly more silicic) lavas on Mars.

5. Discussion

[37] The emplacement times in Table 11 are all within the realm of what would be expected for flows of the sizes considered, based on terrestrial experience. Despite the broad range of flow sizes and emplacement times, the bulk viscosities of the erupted lavas are all very similar. If one assumes only conductive cooling (which is realistic and appropriate for laminar flows), the predicted dynamic viscosities for all but one of the flows (Pavonis West) are $\sim 10^6$ Pa s. The calculated bulk viscosity of the Pavonis West flow is about 1 order of magnitude less than the other five flows. Keeping in mind that the bulk viscosity is an effective viscosity that includes the effect of the crust, this range of 10^5–10^6 Pa s is well within the 10^2–10^7 Pa s range of values reported for terrestrial basaltic lavas [e.g., *Walker*, 1967; *Lipman and Banks*, 1987; *Moore*, 1987; *Crisp et al.*, 1994; *Hon et al.*, 2003]. These results for emplacement time and lava viscosity provide additional support to the conclusions of *Baloga and Glaze* [2008] that the long leveed lava flows on Mars are similar to terrestrial flows, requiring only modest extrapolation.

[38] Using the hybrid approach, emplacement times of about 1–10 years for the six flows examined here are constrained by the time it takes to cool the crust. To illustrate the integrity of these constraints, a limited error analysis has been completed for the emplacement times and other results in Table 11. Because there is so much uncontrolled variability in the emplacement process, it is not possible to perform a complete rigorous error analysis. However, some sources of variability can be estimated and propagated for the final results. Table 1 shows that dispersions in the measured data of 10–20% are typical. An estimate of the cumulative uncertainty is obtained by adding the individual dispersions of the dimensional measurements (h, w_{co}, w_{ci}, and w) in quadrature. Inclusion of an additional 10–15% dispersion due to the use of the conductive cooling relation leads to an approximate overall combined dispersion of $\sqrt{(5 \times 0.15^2)} = 34\%$ in the emplacement times. Uncertainty limits for the other results in Table 11 can be obtained by using multiplicative error models and the individual and combined dispersions in the original formu-

Table 2. Detailed Measurement Data for Flow 1 Determined From Gridded MOLA Data[a]

	Distance (km)	h_l (m)	w (km)	w_{co} (km)	w_{ci} (km)
Profile					
1	0	**13**	**36.4**	**30.4**	5.8
2	16.0	29	33.0	19.5	9.3
3	32.6	36	32.7	17.8	6.6
4	52.9	36	45.4	23.1	10.6
5	73.0	39	39.4	23.8	13.2
6	98.8	**33**	**17.3**	**6.0**	5.6
7	120.7	**42**	**28.3**	**6.8**	3.7
8	138.9	19	29.8	16.8	7.4
9	159.7	28	28.3	15.6	4.9
10	168.9	**32**	**25.4**	**10.1**	10.1
11	189.5	**26**	**19.9**	**9.8**	6.5
12	212.2	26	31.2	21.4	17.2
13	232.2	32	21.1	11.8	7.9
14	258.6	32	42.5	27.4	10.6
15	284.0	**29**	**44.7**	**35.7**	13.9
16	307.3	**30**	**41.2**	**30.3**	13.9
Mean (m)		31	33.7	19.7	9.2
Standard deviation (m)		6	7.6	4.8	3.8
Number of points used in average		9	9	9	16
Uncertainty (2 × standard error on the mean, m)		4	5.0	3.2	1.9

[a]See Figure 7b for profile locations. Boldface values indicate locations along the flow where the relationship in equation (6) does not hold. These cells have been excluded in calculations of the mean, standard deviation and standard error on the mean.

Table 3. Detailed Measurement Data for Flow 2 Determined From Gridded MOLA Data[a]

	Distance (km)	h_l (m)	w (km)	w_{co} (km)	w_{ci} (km)
Profile					
22	0	**31**	**17.1**	**6.3**	6.3
21	5.5	36	17.1	10.8	10.8
20	12.3	**31**	**17.1**	**8.1**	8.1
19	19.2	32	18.9	9.9	5.4
18	29.7	47	18.9	10.8	3.6
17	40.7	**35**	**14.4**	**7.2**	7.2
16	49.7	35	22.5	12.6	5.4
15	57.1	46	19.8	11.7	6.3
14	65.3	45	18.9	10.8	3.6
13	74.1	**48**	**18.0**	**6.3**	5.4
12	84.0	**48**	**32.4**	**13.5**	8.1
11	93.4	49	25.2	16.2	16.2
10	102.5	62	29.7	18.0	9.0
9	109.7	53	24.3	13.5	7.2
8	118.7	61	26.1	17.1	7.2
7	126.8	**62**	**28.8**	**14.4**	9.9
6	133.1	60	27.9	18.9	10.8
5	145.9	57	27.9	15.3	7.2
4	154.0	46	36.0	20.7	9.0
3	160.4	48	35.1	23.4	9.9
2	167.6	50	39.6	23.4	12.6
1	173.0	49	39.6	27.9	12.6
Mean (m)		49	26.7	16.3	8.3
Standard deviation (m)		10	7.7	5.5	3.1
Number of points used in average		16	16	16	22
Uncertainty (2 × standard error on the mean, m)		5	3.8	2.8	1.3

[a]See Figure 7b for profile locations. Boldface values indicate locations along the flow where the relationship in equation (6) does not hold. These cells have been excluded in calculations of the mean, standard deviation and standard error on the mean.

las used to obtain the results. A multiplicative model typically leads to a lognormal (asymmetric) distribution. At the simplest level of analysis, the propagated uncertainty limits for the values shown in Table 11 range from 25% lower to 50% higher for the advance rates and channel velocities, 65% lower and a factor of 2 higher for viscosity, and 45% lower to a factor of 2 higher for the effusion rates. Although there are undoubtedly unrecognized systematic factors and errors that cannot be quantified, the results and uncertainties in Table 11 represent a substantial improvement over previously existing constraints that could be uncertain by as much as several orders of magnitude.

[39] Perhaps the most important result of this study is that the volumetric effusion rates (Table 11) associated with these flows are well within the range of terrestrial examples for historic long-lived eruptions. The three flows near Arsia Mons (flows 4–6) all have effusion rates <100 m^3 s^{-1}. Even the three larger lava flows (Pavonis West, Pavonis East, and Alba Upper) have effusion rates <1000 m^3 s^{-1}, as possibly occurred during the peaks of the Mauna Loa (1950), Hualalai (1801) and Kilauea Great Crack (1823) eruptions [*Malin*, 1980; *Rowland and Walker*, 1990; *Baloga et al.*, 1995]. However, the primary difference between the estimated eruption rates in Table 11 and terrestrial experience is the duration over which these high eruption rates must have been maintained.

[40] The flows in Table 11 are listed in order of decreasing effusion rate. The flows on the plains north of Pavonis Mons show the highest effusion rates, whereas the flows on the flanks of Arsia Mons all show much lower effusion rates. Flows 1–3 are all on somewhat lower slopes than flows 4–6, but the effusion rate does not appear to be directly correlated with slope. Emplacement times for these six flows vary over an order of magnitude. From this, one might conclude that although all six flows are of similar "size" (lengths and thicknesses), the eruptions that fed flows 4, 5, and 6 are somehow fundamentally different. The lavas in all six flows have similar calculated viscosities, but the effusion rates from the vents that fed the Arsia North, Arsia Southeast, and Arisa Southwest are substantially lower than those that must have driven the emplacement of the larger volume (i.e., wider) flows on the plains north of Pavonis Mons and on the southwestern flanks of Alba Patera.

[41] As a note, the emplacement time and effusion rate for the Pavonis East flow is different from that originally reported by *Baloga and Glaze* [2008]. The work presented here has used identically the same outer channel and levee

Table 4. Detailed Measurement Data for Proximal Portion of Flow 3 Determined From Individual MOLA PEDR Data[a]

	MOLA PEDR	Distance (km)	h_l (m)	w (km)	w_{co} (km)	w_{ci} (km)
Profile						
16	16876	0	20	11.4	7.9	5.8
15	13581	2.1	**30**	**6.6**	**3.0**	2.2
14	10940	14.9	30	9.0	5.5	3.0
13	12424	19.2	30	10.2	6.7	4.2
12	11682	26.7	20	9.4	5.9	3.4
11	20194	32.4	23	9.7	6.2	5.3
10	17995	41.6	**24**	**16.7**	**13.2**	6.3
9	19792	48.7	**35**	**16.0**	**12.5**	6.6
8	1685	53.0	**35**	**15.0**	**11.5**	7.0
Mean (m)			25	9.9	6.4	4.9
Standard deviation (m)			5	0.9	0.9	1.7
Number of points used in average			5	5	5	9
Uncertainty (2 × standard error on the mean, m)			5	0.8	0.8	1.2

[a]See Figure 1 for profile locations. Boldface values indicate locations along the flow where the relationship in equation (6) does not hold. These cells have been excluded in calculations of the mean, standard deviation and standard error on the mean.

Table 5. Detailed Measurement Data for Distal Portion of Flow 3 Determined From Individual MOLA PEDR Data[a]

Profile	MOLA PEDR	Distance (km)	h_l (m)	w (km)	w_{co} (km)	w_{ci} (km)
7	11921	0	40	14.4	10.0	4.5
6	18347	6.4	35	14.1	9.0	5.0
5	19390	13.9	**45**	**14.3**		
4	16612	20.3	**47**	**11.7**	**8.5**	**5.0**
3	17291	28.1	**35**	**9.0**	**7.0**	**4.0**
2	1591	40.2	**46**	**6.9**	**5.8**	**3.5**
1	14713	48.4	**46**	**6.6**	**5.5**	**3.5**

[a]See Figure 1 for profile locations. Boldface values indicate locations along the flow where the relationship in equation (6) does not hold. This portion of flow 3 (Alba) is not included in the hybrid model analysis (see text for explanation).

Table 6. Detailed Measurement Data for Flow 4 Determined From Individual MOLA PEDR Data[a]

	MOLA PEDR	Distance (km)	h_l (m)	w (km)	w_{co} (km)	w_{ci} (km)
Profile						
1	14027	0	17	4.9	2.7	1.8
2	13285	24.6	12	5.5	3.4	2.1
3	18667	38.4	28	4.9	3.0	1.2
4	13612	59.2	19	3.0	1.8	1.2
5	14920	62.6	29	4.0	2.2	1.2
6	16907	63.8	31	5.5	3.7	1.8
7	13939	74.5	27	4.9	3.4	1.5
Mean (m)			23	4.7	2.9	1.5
Standard deviation (m)			7	0.9	0.7	0.4
Number of points used in average			7	7	7	7
Uncertainty (2 × standard error on the mean, m)			5	0.7	0.5	0.3

[a]See Figure 7c for profile locations.

dimensions, as well as the same self-replication model, exactly as described by *Baloga and Glaze* [2008]. However, an error in the code used for that paper resulted in an erroneous determination of 8 m of crust required to make the levees. This error propagated through to an estimate of 600 days for emplacement (assuming conduction only) and an eruption rate of 2250 $m^3\ s^{-1}$. The corrected values are as follows: 17m crust; 2,700 days; and 875 $m^3\ s^{-1}$ eruption rate at the source. For comparison, by allowing the levees to continue to grow after the flow front has passed, using the hybrid model discussed here, the effusion rate at the source decreases from 875 $m^3\ s^{-1}$ to 840 $m^3\ s^{-1}$, and the viscosity increases slightly (2.8×10^6 Pa s to 3.1×10^6 Pa s).

Table 7. Detailed Measurement Data for Distal Portion of Flow 5 Determined From Gridded MOLA Data[a]

	Distance (km)	h_l (m)	w (km)	w_{ci} (km)
Measurement				
1	0	-	1.5	-
2	10	-	1.5	-
3	20	-	3.1	-
4	30	-	2.0	0.7
5	40	-	2.3	0.6
6	50	-	4.0	1.0
7-left	53	11	-	-
7-right	53	22	-	-
8	60	-	2.5	1.0
9	70	-	3.5	0.8
10	80	-	3.8	1.0
11	90	-	2.8	1.2
12	100	-	5.4	1.2
13	110	-	3.5	1.5
14	116	-	5.9	1.2
15	120	-	4.4	-
16-left	129	26	-	-
17	130	-	6.6	-
18	140	-	5.5	-
19	146	-	3.3	-
Mean (m)		20	3.6	1.0
Standard deviation (m)		8	1.5	0.3
Number of points used in average		3	17	10
Uncertainty (2 × standard error on the mean, m)		4	0.7	0.2

[a]See Figure 7d for profile locations.

Table 8. Detailed Measurement Data for Distal Portion of Flow 6 Determined From Gridded MOLA Data[a]

	Distance (km)	h_l (m)	w (km)	w_{ci} (km)
Profile				
1	0	-	1.7	0.3
2	10	-	2.0	0.5
3	20	-	1.9	0.5
4-left	23	22	-	-
4-right	23	26	-	-
5	30	-	3.0	0.5
6	40	-	2.5	0.8
7	50	-	2.8	0.7
8	60	-	3.4	0.8
9	70	-	4.4	0.9
10	80	-	3.3	0.7
11	90	-	3.3	1.2
12-left	95	20	-	-
12-right	95	17	-	-
13	100	-	6.0	1.8
14	105	-	9.0	2.0
15	110	-	6.5	-
16	120	-	12.1	-
17	130	-	9.7	-
18-left	134	45	-	-
18-right	134	36	-	-
19	140	-	5.3	-
20	150	-	6.4	-
21	158	-	2.3	-
Mean (m)		28	4.7	0.9
Standard deviation (m)		11	3.0	0.5
Number of points used in average		6	18	12
Uncertainty (2 × standard error on the mean, m)		4	1.4	0.3

[a]See Figure 7e for profile locations.

[42] Lava compositions ranging from basalt to basaltic andesites are admissible by this analysis. Terrestrial lava flows with such compositions are well known to produce channelized flows with stationary levees [e.g., *Moore*, 1987; *Linneman and Borgia*, 1993; *Thordarson and Larsen*, 2007]. Furthermore, field estimates of viscosities for basaltic andesites overlap with basalts at the higher end of the range (e.g., 10^5–10^6 Pa s) [*Walker*, 1973].

[43] The suggestion that these Martian flows are basaltic to basaltic andesite in composition is consistent with, and a refinement of, prior theoretical estimates [e.g., *Zimbelman*, 1985; *Hiesinger et al.*, 2007]. More recently, Mars Pathfinder, and Mars Exploration Rover (MER) landing site analyses have also detected basaltic to andesitic compositions [*Rieder et al.*, 1997; *McSween et al.*, 1999, 2004; *Greeley et al.*, 2005]. Many of the channelized lava flows

Table 9. Comparison of Levee Width Ratio With Channel Width Ratio

	w_{lo}/w_{li}	w_{ci}/w_{co}
Pavonis West (flow 1)	0.61	0.47
Pavonis East (flow 2)	0.61	0.51
Alba (Upper) (flow 3)	0.53	0.76
Arsia North (flow 4)	0.57	0.53
Average	0.58	0.57
Standard deviation	0.04	0.13

Table 10. Calculated Crust Thicknesses Using Individual Profile Data and Average Flow Dimensions[a]

Flow	Name	Crust Thickness (m)	
		Full Data	Averaged Dimensions
1	Pavonis West	17	16
2	Pavonis East	21	20
3	Alba (Upper)	7	7
4	Arsia North	9	9
5	Arsia Southeast	-	11
6	Arsia Southwest	-	23

[a]Only averaged dimensions were used for flows 5 and 6.

on the flanks of Ascraeus Mons have estimated viscosities on the order of our results here for the plains flows in different regions [*Hiesinger et al.*, 2007]. However, the slopes on the flanks of Ascraeus Mons are an order of magnitude higher than the plains, and the inferred effusion rates are somewhat higher for the large flows on the plains near Pavonis Mons and Alba Patera than found by *Hiesinger et al.* [2007] for the Ascraeus Mons flank flows. Thus, although the calculated viscosities in both settings are comparable, the primary difference is the extended duration of emplacement for the plains flows.

[44] Cross-flow topographic profiles of the leveed flows on the plains of Mars are highly variable [e.g., *Zimbelman*, 1985; *Mouginis-Mark and Yoshioka*, 1998; *Baloga et al.*, 2003; *Glaze et al.*, 2003; *Hiesinger et al.*, 2007; *Baloga and Glaze*, 2008]. In addition, with current imaging data it is often difficult to distinguish levee deposition by the front versus subsequent upstream stagnations, overspills, and inward growth. The theory described here could, in principle, be readily modified to account for the fine-scale shape of inner and outer levee deposition. However, owing to the large influence of natural random effects in the emplacement of leveed flows on the Mars plains and the basic level of physics in the current theory, such effort does not appear warranted at this time. Even with improved imaging data, more meaningful insight about emplacement dynamics would be obtained from the statistical characterization of the random influences on individual flows and interregional differences, than by detailed study of inner and outer levee morphologies.

6. Conclusions

[45] Observations of terrestrial lava flows and laboratory experiments have motivated the development of a hybrid model for the emplacement of channelized lava flows. This hybrid model combines two end-member processes for levee formation. The first process deposits lava into levees at the flow front in the Distal Zone. The volume of lava transferred into the levees is derived from the excess volume flow rate in the upper portion of the fluid core as well as from any overriding crust. The second process adds to these initial levees in an Intermediate Zone through inward growth and overspills after the flow front has passed. The hybrid model assumes that the levee growth eventually stabilizes such that the upstream channel in the Stationary Zone is in a steady state condition. In almost all the flows examined here, there is some evidence of transient stagnation, interruption of continuous lava supply, or a breakout/overspill that diverted lava from the steady, continuous channel flow concept of the model. While such factors cannot be estimated from the deposit dimensions and morphology, the model presented here provides the most reasonable method presently available for estimating the large-scale average features (e.g., emplacement time, advance velocity) of the emplacement.

[46] The dimensions of outer levees, as seen in topographic profile data, are used as input for the formation of levees in the Distal Zone, and constrain the thickness of crust that must have been deposited into the levees at the flow front. From the crust thickness, an independent constraint on the emplacement time can be found by estimating the time it would take to conductively cool lava to the solidus temperature.

[47] The volume of material contained in the inner levees (total levee volume less the outer levee volume) can then be used to constrain the difference between the average advance rate of the flow front, and the upstream steady state velocity of the fluid core. Lava viscosities and eruption rates are determined on the basis of the inner channel dimensions and lava velocity in the Stationary Zone. Crustal thicknesses for the six flows examined range from 9 to 23 m, consistent with various terrestrial values reported by *Baloga and Glaze* [2008]. The emplacement times required to obtain these crust thicknesses range from about 1 year to 10 years. Corresponding viscosities for five of the six flows are on the order of 10^6 Pa s, with Pavonis West about 1/3 that value. Effusion rates range from 25 to 840 $m^3\ s^{-1}$, and are all within the range of terrestrial experience.

[48] The three Arsia Mons flank flows all have predicted effusion rates substantially lower than the flows near Pavonis Mons and Alba Patera, despite all having very similar lava viscosities. The eruptions in this region near Arsia Mons may have resulted from a significantly different plumbing system or subsurface ambient conditions.

[49] The results here continue to support the conclusions of *Baloga and Glaze* [2008] that large channelized flows on Mars are similar to terrestrial flows, except for the much longer eruption durations on Mars. The analysis presented here is thus suggestive of significant differences in the

Table 11. Results for Emplacement Time and Viscosity Using the Hybrid Model for Leveed Lava Flows

Flow	Name	Emplacement Time (Earth years)	Advance Rate ($cm\ s^{-1}$)	Channel Velocity ($cm\ s^{-1}$)	Viscosity (10^6 Pa s)	Effusion Rate ($m^3\ s^{-1}$)
1	Pavonis West	4.8	0.20	0.30	0.3	840
2	Pavonis East	7.4	0.07	0.10	3.1	414
3	Alba (Upper)	0.9	0.19	0.26	3.6	306
4	Arsia North	1.4	0.16	0.24	3.5	84
5	Arsia Southeast	2.1	0.22	0.34	1.2	67
6	Arsia Southwest	9.5	0.05	0.10	1.0	25

sources of magma supply on Mars as well as regional differences among the volcanic provinces.

Notation

G Gravity, m s^{-2}.
h_c Fluid core thickness, m.
h_l Total flow thickness, m.
L Flow front location, m.
Q Volume flow rate, m^3 s^{-1}.
Q_{ex} Total excess volume flow rate, m^3 s^{-1}.
$Q_{ex:core}$ Excess volume flow rate of the core, m^3 s^{-1}.
$Q_{ex:crust}$ Excess volume flow rate of the crust, m^3 s^{-1}.
t Time, s.
u_c Velocity of the fluid core, m s^{-1}.
$\bar{u}_c$ Average velocity of the fluid core, m s^{-1}.
u_f Average advance rate of the flow front, m s^{-1}.
w Total flow width, m.
w_c Channel width, m.
w_{ci} Inner channel width, m.
w_{co} Outer channel width, m.
w_l Levee width, m.
w_{li} Inner levee width, m.
w_{lo} Outer levee width, m.
w_∞ Final levee width, m.
x Horizontal distance coordinate, m.
z Vertical distance coordinate, m.
Γ Time constant for inward levee growth, s.
μ Dynamic viscosity, Pa s.
θ Slope, deg.
ρ Density, kg m^{-3}.

[50] **Acknowledgments.** The authors would like to thank Laszlo Keszthelyi and an anonymous reviewer for helpful suggestions for improving this manuscript. Support for this work was provided by the NASA Mars Data Analysis Program through grants NAG5–13348 (S.A.F. and C.P.) and NNX06AD98G (S.M.B.) and RTOP support for L. Glaze.

References

Bailey, J. E., A. J. L. Harris, J. Dehn, S. Calvari, and S. K. Rowland (2006), The changing morphology of an open lava channel on Mt. Etna, *Bull. Volcanol.*, *68*, 479–515, doi:10.1007/s00445-005-0025-6.

Baloga, S. (1987), Lava flows as kinematic waves, *J. Geophys. Res.*, *92*, 9271–9279, doi:10.1029/JB092iB09p09271.

Baloga, S. M., and L. S. Glaze (2008), A self-replication model for long channelized lava flows on the Mars plains, *J. Geophys. Res.*, *113*, E05003, doi:10.1029/2007JE002954.

Baloga, S. M., P. D. Spudis, and J. E. Guest (1995), The dynamics of rapidly emplaced terrestrial lava flows and implications for planetary volcanism, *J. Geophys. Res.*, *100*, 24,509–24,519, doi:10.1029/95JB02844.

Baloga, S., L. S. Glaze, J. A. Crisp, and S. A. Stockman (1998), New statistics for estimating the bulk rheology of active lava flows: Puu Oo examples, *J. Geophys. Res.*, *103*, 5133–5142, doi:10.1029/97JB03743.

Baloga, S. M., P. J. Mouginis-Mark, and L. S. Glaze (2003), Rheology of a long lava flow at Pavonis Mons, Mars, *J. Geophys. Res.*, *108*(E7), 5066, doi:10.1029/2002JE001981.

Blake, S., and B. C. Bruno (2000), Modeling the emplacement of compound lava flows, *Earth Planet. Sci. Lett.*, *184*, 181–197, doi:10.1016/S0012-821X(00)00278-8.

Carr, M. H. (1974), The role of lava erosion in the formation of lunar rilles and Martian channels, *Icarus*, *22*, 1–23, doi:10.1016/0019-1035(74)90162-6.

Cashman, K. V., R. C. Kerr, and R. W. Griffiths (2006), A laboratory model of surface crust formation and disruption on lava flows through non-uniform channels, *Bull. Volcanol.*, *68*, 753–770, doi:10.1007/s00445-005-0048-z.

Crisp, J. A., and S. M. Baloga (1990), A model for lava flows with two thermal components, *J. Geophys. Res.*, *95*, 1255–1270, doi:10.1029/JB095iB02p01255.

Crisp, J. A., K. V. Cashman, J. A. Bonini, S. B. Hougen, and D. C. Pieri (1994), Crystallization history of the 1984 Mauna Loa lava flow, *J. Geophys. Res.*, *99*, 7177–7198, doi:10.1029/93JB02973.

Fink, J. H., and R. W. Griffiths (1990), Radial spreading of viscous-gravity currents with solidifying crust, *J. Fluid Mech.*, *221*, 485–509, doi:10.1017/S0022112090003640.

Garry, W. B. (2006), The emplacement of channeled flows in subaerial, submarine, simulated, and extraterrestrial environments, Ph.D. dissertation, 240 pp., State Univ. of New York at Buffalo, Buffalo.

Garry, W. B., and J. R. Zimbelman (2007), Morphology and emplacement of long lava flows in the Tharsis Volcanic Province, Mars, *Eos Trans. AGU*, *88*(23), Jt. Assem. Suppl., Abstract P34A–04.

Garry, W. B., T. K. P. Gregg, S. A. Soule, and D. J. Fornari (2006), Formation of submarine lava channel textures: Insights from laboratory simulations, *J. Geophys. Res.*, *111*, B03104, doi:10.1029/2005JB003796.

Garry, W. B., J. R. Zimbelman, and T. K. P. Gregg (2007), Morphology and emplacement of a long channeled lava flow near Ascraeus Mons volcano, Mars, *J. Geophys. Res.*, *112*, E08007, doi:10.1029/2006JE002803.

Glaze, L. S., and S. Baloga (1998), Dimensions of Pu'u O'o lava flows on Mars, *J. Geophys. Res.*, *103*, 13,659–13,666.

Glaze, L. S., and S. M. Baloga (2006), Rheologic inferences from the levees of lava flows on Mars, *J. Geophys. Res.*, *111*, E09006, doi:10.1029/2005JE002585.

Glaze, L. S., and S. M. Baloga (2007), Topographic variability on Mars: Implications for lava flow modeling, *J. Geophys. Res.*, *112*, E08006, doi:10.1029/2006JE002879.

Glaze, L. S., S. Baloga, and E. R. Stofan (2003), A methodology for constraining lava flow rheologies with MOLA, *Icarus*, *165*, 26–33, doi:10.1016/S0019-1035(03)00171-4.

Greeley, R., B. H. Foing, H. Y. McSween Jr., G. Neukum, P. Pinet, M. van Kan, S. C. Werner, D. A. Williams, and T. E. Zegers (2005), Fluid lava flows in Gusev crater, Mars, *J. Geophys. Res.*, *110*, E05008, doi:10.1029/2005JE002401.

Gregg, T. K. P., and J. H. Fink (1995), Quantification of submarine lava-flow morphology through analog experiments, *Geology*, *23*, 73–76, doi:10.1130/0091-7613(1995)023<0073:QOSLFM>2.3.CO;2.

Gregg, T. K. P., and J. H. Fink (1996), Quantification of extraterrestrial lava flow effusion rates through laboratory simulations, *J. Geophys. Res.*, *101*, 16,891–16,900, doi:10.1029/96JE01254.

Griffiths, R. W., K. C. Kerr, and K. V. Cashman (2003), Patterns of solidification in channel flows with surface cooling, *J. Fluid Mech.*, *496*, 33–62, doi:10.1017/S0022112003006517.

Guest, J. E., C. R. J. Kilburn, H. Pinkerton, and A. M. Duncan (1987), The evolution of lava flow-fields: Observations of the 1981 and 1983 eruptions of Mount Etna, Sicily, *Bull. Volcanol.*, *49*, 527–540, doi:10.1007/BF01080447.

Guest, J. E., P. D. Spudis, R. Greeley, G. J. Taylor, and S. M. Baloga (1995), Emplacement of xenolith nodules in the Kaupulehu lava flow, Hualalai Volcano, Hawaii, *Bull. Volcanol.*, *57*, 179–184.

Hiesinger, H., J. W. Head III, and G. Neukum (2007), Young lava flows on the eastern flank of Ascraeus Mons: Rheological properties derived from High Resolution Stereo Camera (HRSC) images and Mars Orbieter Laser Altimeter (MOLA) data, *J. Geophys. Res.*, *112*, E05011, doi:10.1029/2006JE002717.

Hon, K., J. Kauahikaua, R. Denlinger, and K. Mackay (1994), Emplacement and inflation of pahoehoe sheet flows: Observations and measurements of active lava flows on Kilauea Volcano, Hawaii, *Geol. Soc. Am. Bull.*, *106*(3), 351–370, doi:10.1130/0016-7606(1994)106<0351:EAIOPS>2.3.CO;2.

Hon, K., C. Gansecki, and J. Kauahikaua (2003), The transistion from 'a'a to pahoehoe crust on flows emplaced during the Pu'u 'O'o-Kupaianaha eruption, *U.S. Geol. Surv. Prof. Pap.*, *1676*, 89–103.

Hulme, G. (1974), The interpretation of lava flow morphology, *Geophys. J. R. Astron. Soc.*, *39*, 361–383.

Kerr, R. C., R. W. Griffiths, and K. V. Cashman (2006), Formation of channelized lava flows on an unconfined slope, *J. Geophys. Res.*, *111*, B10206, doi:10.1029/2005JB004225.

Linneman, S. R., and A. Borgia (1993), The blocky andesitic lava flows of Arenal volcano, Costa Rica, in *Active Lavas*, edited by R. J. Kilburn and G. Luongo, pp. 25–72, Routledge, London.

Lipman, P. W., and N. G. Banks (1987), AA flow dynamics, Mauna Loa 1984, in *Volcanism in Hawaii*, edited by R.W. Decker et al., *U.S. Geol. Surv. Prof. Pap.*, vol. 1350, pp. 1527–1567.

Malin, M. C. (1980), Lengths of Hawaiian lava flows, *Geology*, *8*, 306–308, doi:10.1130/0091-7613(1980)8<306:LOHLF>2.0.CO;2.

McSween, H. Y., et al. (1999), Chemical, multispectral, and textural constraints on the composition and origin of rocks at the Mars Pathfinder landing site, *J. Geophys. Res.*, *104*, 8679–8715, doi:10.1029/98JE02551.

McSween, H. Y., et al. (2004), Basaltic rocks analyzed by the Spirit rover in Gusev crater, *Science*, *305*, 842–845, doi:10.1126/science.3050842.

Moore, H. J. (1987), Preliminary estimates of the rheological properties of 1984 Mauna Loa lava, in *Volcanism in Hawaii*, edited by R.W. Decker et al., in *U.S. Geol. Surv. Prof. Pap.*, *1350*, 1569–1588.

Mouginis-Mark, P. J., and M. T. Yoshioka (1998), The long lava flows of Elysium Planitia, Mars, *J. Geophys. Res.*, *103*, 19,389–19,400.

Rieder, R., T. Economou, H. Wanke, A. Turkevich, J. Crisp, J. Bruckner, G. Dreibus, and H. Y. McSween (1997), The chemical composition of Martian soil and rocks returned by the mobile alpha proton X-ray spectrometer: Preliminary results from the X-ray mode, *Science*, *278*, 1771–1774, doi:10.1126/science.278.5344.1771.

Rossi, M. J. (1997), Morphology of the 1984 open-channel lava flow at Krafla volcano, northern Iceland, *Geomorphology*, *20*, 95–112, doi:10.1016/S0169-555X(97)00007-X.

Rowland, S. K., and G. P. L. Walker (1990), Pahoehoe and aa in Hawaii: Volumetric flow rate controls the lava structure, *Bull. Volcanol.*, *52*, 615–628, doi:10.1007/BF00301212.

Rowland, S. K., A. J. L. Harris, and H. Garbeil (2004), Effects of Martian conditions on numerically modeled, cooling-limited channelized lava flows, *J. Geophys. Res.*, *109*, E10010, doi:10.1029/2004JE002288.

Smith, D. E., et al. (2001), Mars Orbiter Laser Altimeter: Experiment summary after the first year of global mapping of Mars, *J. Geophys. Res.*, *106*, 23,689–23,722, doi:10.1029/2000JE001364.

Thordarson, T., and G. Larsen (2007), Volcanism in Iceland in historical time: Volcano types, eruption styles and eruptive history, *J. Geodyn.*, *43*, 118–152, doi:10.1016/j.jog.2006.09.005.

Walker, G. P. L. (1967), Thickness and viscosity of Etnean lavas, *Nature*, *213*(5075), 484–485, doi:10.1038/213484a0.

Walker, G. P. L. (1973), Lengths of lava flows, *Philos. Trans. R. Soc. London, Ser. B*, *274*, 107–118.

Zimbelman, J. (1985), Estimates of rheologic properties for flows on the Martian volcano Ascraeus Mons, *Proc. Lunar Planet. Sci. Conf. 16th*, Part 1, *J. Geophys. Res.*, *90*, suppl., D157–D162.

S. M. Baloga, Proxemy Research, 20528 Farcroft Lane, Gaithersburg, MD 20882, USA. (Steve@proxemy.com)

S. A. Fagents and C. Parcheta, Hawaii Institute for Geophysics and Planetology, University of Hawaii at Mānoa, 1680 East-West Road, POST 602, Honolulu, HI 96822, USA. (fagents@higp.hawaii.edu; parcheta@hawaii.edu)

W. B. Garry, Center for Earth and Planetary Studies, National Air and Space Museum, Smithsonian Institution, MRC 315, P.O. Box 37012, Washington, DC 20013-7012, USA. (GarryW@si.edu)

L. S. Glaze, NASA Goddard Space Flight Center, Code 698, Greenbelt, MD 20771, USA. (Lori.S.Glaze@nasa.gov)